Design, construction and traceable calibration of a phosphor-based fibre-optic thermometer from 0 °C to 650 °C

To cite this article: D Lowe *et al* 2021 *Meas. Sci. Technol.* **32** 094004

View the article online for updates and enhancements.

You may also like

- A summary of new developments in phosphor thermometry
  Frank Beyrau, Benoît Fond and Christopher Abram

- Comparison of lifetime-based methods for 2D phosphor thermometry in high-temperature environment
  Di Peng, Yingzheng Liu, Xiaofeng Zhao et al.

- Meta-study of laser power calibrations ranging 20 orders of magnitude with traceability to the kilogram
  Paul A Williams, Matthew T Spidell, Joshua A Hadler et al.

Design, construction and traceable calibration of a phosphor-based fibre-optic thermometer from 0 °C to 650 °C

D Lowe* , G Sutton , A Sposito, G Machin and J Pearce

Thermal and Radiometric Metrology, National Physical Laboratory, Teddington, United Kingdom

E-mail: dave.lowe@npl.co.uk

CrossMark

Abstract

Measurement traceability, in which there is a documented chain of calibration links from a measurement back to a primary realisation of a unit, is vital for achieving the smallest uncertainty in metrology. A sensor that can provide a traceable link in harsh environments may be advantageous even if its uncertainty is larger than that of typical calibrated devices. A phosphor-based thermometer that has optical rather than electrical connections has been built and then calibrated in terms of the International Temperature Scale of 1990. Its standard uncertainty ranges from 0.5 °C at 0 °C to 2 °C at 650 °C. While this uncertainty cannot match what is possible with thermocouples or resistance thermometers, the optical basis of the sensor means it can be used in situations where electrical connections are precluded.

1. Introduction

Temperature measurement with conventional electrical sensors such as thermocouples and resistance thermometers can be adversely affected and degraded when operated in harsh environments. Sensors can be perturbed by electromagnetic fields and damaged via transmutation when exposed to gamma or neutron fluxes. Non-electrical sensors based on optical phenomena such as radiance, phosphorescence, reflectance and interference have the potential to overcome these challenges. By using optical fibres for such sensors, the conversion of optical to electrical signals and the subsequent signal processing that is normally required can be performed remotely away from the harsh environment. In principle, due to their excellent optical transmission properties, the stand-off distance can be large and in some cases as great as several kilometres making these sensors ideally suited to large industrial environments. Fibre optic sensors are already available with Fabry–Pérot interferometers and fibre Bragg gratings providing specific location measurement and distributed systems that use Rayleigh or Raman scattering along the length of the fibre.

Systems such as the Luxtron/Accufiber and ASEA use the temperature-dependent luminescence of a small sample placed at the end of an optical fibre as a contact thermometer [1]. Conventional fibres are temperature limited to around 130 °C due to their protective polymer coating that prevents contamination of the silica cladding and core which might otherwise devitrify. Fibres coated in metals are available and a phosphor-based fibre optic probe based on four 400 μm gold coated fibres was reported by Grattan *et al* [2] that operated

---

up to around 550 °C, although with limited sensitivity above 500 °C.

As part of the Euramet EMPIR funded project EMPRESS2 [3], we have developed and validated a fibre optic temperature contact sensor that is suitable for use in harsh environments; specifically, the aim was to develop, calibrate and test a novel phosphor tipped single fibre thermometer for use up to 650 °C that has an uncertainty less than 5 °C. This paper describes the thermometer, its characterisation and calibration traceable to ITS-90, the International Temperature Scale of 1990 [4].

1.1. Principle of phosphor thermometry

Phosphor thermometry [5, 6] relies on photoluminescence— the emission of light at one wavelength caused by excitation at a different wavelength—where the luminescence has a temperature dependence. It has application in, for example, combustion thermometry [7], surface temperature measurement [8] and thermometry of gas and liquid flows [9]. In phosphor thermometry, there are two main methods in use to evaluate temperature: decay time and intensity ratio.

1.1.1. Decay time. An activator in the luminescent material absorbs a photon from an excitation source, enters into an excited state and then loses that extra energy by a mixture of radiative emission and thermalisation (i.e. via photons and phonons). The activator therefore emits at a longer wavelength than the absorption. Depending on the persistence time in the excited state, the emission intensity decays exponentially after the excitation is switched off. Thermometry applications take advantage of phosphors where the phosphor decay varies monotonically over the temperature range of interest. The decay can either be measured directly or as a phase difference between a periodically varying excitation and the corresponding emission [6].

1.1.2. Ratio. Some phosphors show multiple spectral features [10], and the relative intensity of these can depend on temperature. As a result, spectral measurement can be used to determine the phosphor temperature. Often a simple ratio between two spectral bands can be used [1]. This can be seen in figure 1 for manganese doped magnesium fluorogermanate (MFG) where the emission amplitude in a band around 660 nm changes more rapidly and, for this temperature range, in the opposite sense—the signal level decreasing rather than increasing—to a band around 630 nm.

2. Instrument design

2.1. Probe design

Silica fibre core and cladding can survive high temperatures well in excess of 650 °C. However, if the fibre is uncoated water vapour and contamination are liable to increase the transformation of silica into cristobalite at higher temperatures [11]. This can change the fibre transmission and bending losses. To protect the fibre at high temperature we used a
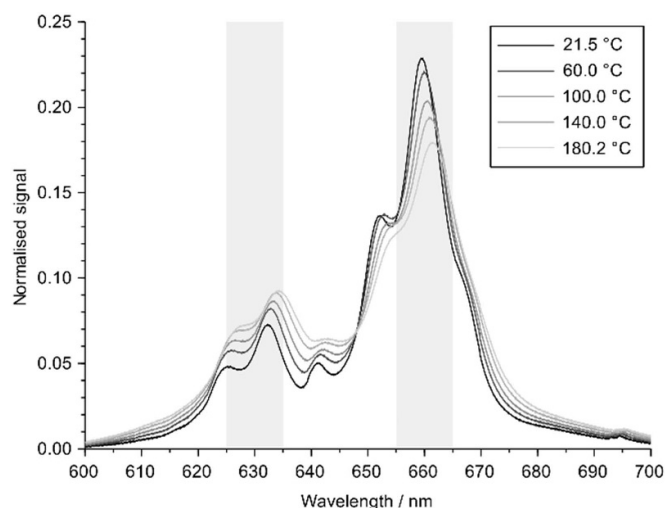

Figure 1. Emission spectra of MFG:Mn at different temperatures when excited with light at 415 nm. The shaded areas indicate spectral regions 10 nm bandwidth centred at 630 nm and 660 nm, which can be seen to have different temperature dependence.

2 m length of gold coated fibre rated to 750 °C [12]. A single fibre was used, with a 400 μm diameter core. With cladding, its diameter is 440 μm and with the gold coating, 510 μm. This single fibre transmits both the excitation light from the source and the emitted light from the sensor.

The phosphor used was manganese doped MFG (MFG:Mn) sourced from Osram. Its temperature-dependent emission when excited with a 415 nm LED is shown in figure 1. The sensor probe was made with the fibre bonded into a 15 mm length of 1.6 mm outer diameter (OD), 0.8 mm inner diameter (ID) alumina tube using Ceramabind 643–1 [13], with nominally 1 mm of the cleaved fibre protruding. This was in turn glued into a 30 mm long alumina tube, 2.7 mm OD and 1.7 mm ID, which was packed with MFG:Mn powder such that the cleaved fibre end was embedded, and then sealed with more Cerambind 643–1.

2.2. Measurement unit

Previous experimental work at NPL indicated we would not be able to reach the high temperature requirement based on the time decay phosphor thermometry technique using a single fibre with the LED excitation and silicon photo-diode detection we wished to use. In particular, the relatively low excitation level from using a fibre coupled LED and the rapid drop in emission at higher temperatures gave low signal levels. The gain of the detectors transimpedence amplifiers was limited by the need to resolve decay curves with a time constant of <1 ms. This combination of low signal and low gain limited the upper temperature to about 525 °C. We therefore designed a system based on the intensity ratio technique, using the ratio of intensity of the two bands of the photoluminescence light defined with band-pass filters centred at 630 nm and 660 nm shown in figure 1.

Figure 2 shows the instrument layout. The 415 nm fibre coupled LED is collimated and passes through a dichroic filter,
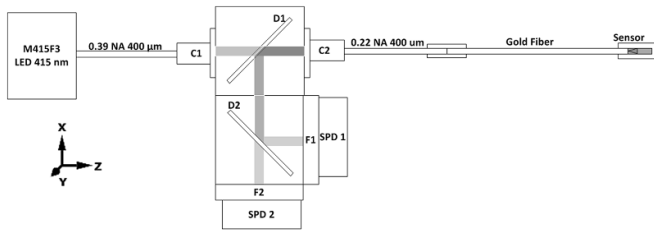
Figure 2. Schematic of the system. The phosphor is excited by a Thorlabs M415F3 fibre coupled LED at nominally 415 nm into a 400 μm fibre. The collimators C1 and C2 are matched to couple the 0.39 numerical aperture (NA) input fibre to the 0.22 NA gold coated fibre.
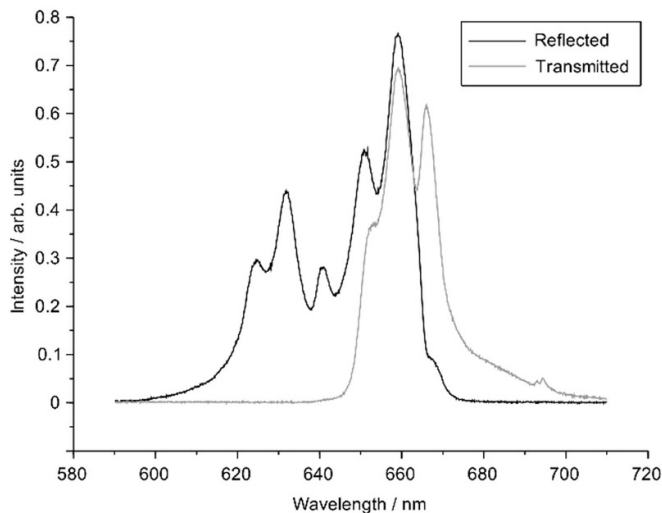

Figure 3. Transmission and reflection of the photoluminescence incident on the 650 nm dichroic filter.

Figure 4. Out-of-band optical rejection of the two channels.

D1, that transmits below 496 nm (>93% transmission from 400 nm to 480 nm and >98% reflectance 512 nm to 900 nm) so that the blue light is directed into the probe fibre collimator, C2. The input collimator C1 can be adjusted for XY so that the signal into C2 is maximised. A length of fibre between C2 and the 2 m long gold-coated fibre can be used to extend the reach of the measurement probe. The 415 nm excitation of the MFG:Mn in the sensor head results in the photoluminescence spectrum of figure 1. This is transmitted back to the measuring unit and is, in turn, collimated by C2. This time the dichroic D1, which transmitted the 415 nm excitation, reflects the longer wavelength red emitted light toward a second dichroic filter.

The second dichroic filter, D2—which transmits wavelengths longer than 650 nm and reflects shorter wavelengths, splits the emitted spectrum as shown in figure 3. This spectrum was measured with a Thorlabs CCS100 spectrometer. The reflected component from D2 is filtered with a 550 nm long pass filter and a 630 nm interference filter that has a bandwidth of 10 nm full width at half maximum (FWHM) (F1). The transmitted component from D2 is similarly filtered with a 550 nm long pass filter and a 660 nm interference filter (F2), also with 10 nm FWHM. The long pass filters reduce any
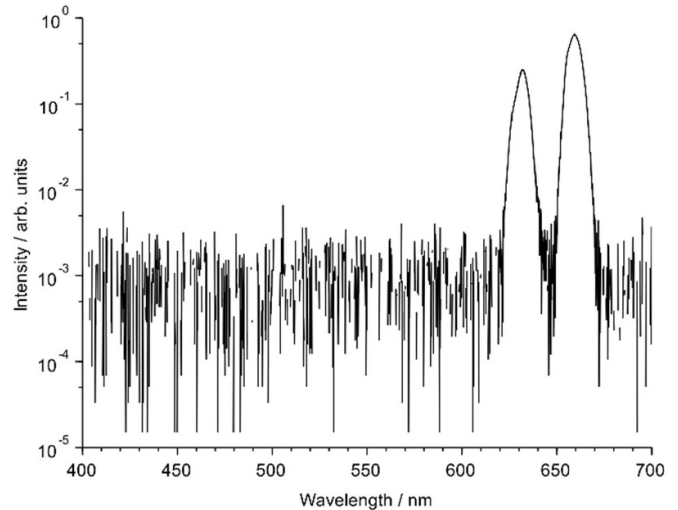
scattered light from the LED that might otherwise contribute to the detector signals. By combining the two channels with a 2×1 fibre coupler, the out-of-band rejection of the reflected and unwanted LED light can be seen to be of the order of 10^3 (figure 4).

Collimator C2 has pitch and yaw adjustment. By iteratively adjusting this together with the X–Y translation adjustment of C1, the signals at the photodiodes SPD1 and SPD2 can be maximised. These are both Hamamatsu S12915-1010 R silicon photodiodes, with a 10 mm by 10 mm sensor. This sensor has higher sensitivity of 0.45 AW^{-1} at 650 nm compared to the 0.35 AW^{-1} of the S1227/S1337 series often used for precision radiometry.

The current signal from each channel is converted to a voltage with a transimpedance amplifier based on an OPA129A opamp with Caddock ultra stable low temperature coefficient resistors giving a gain for each channel of 10^7 VA^{-1}, 10^8 VA^{-1} or 10^9 VA^{-1}.

The output from the amplifiers is connected to two of the analogue inputs of an NI 6356-USB DAQ unit. The same unit provides the analogue square wave for the LED driver. A LabVIEW program runs the system and calculates temperature from the input voltage ratio based on calibration.

2.3. Operation

The LED is powered with a 1 Hz square wave. The square wave excitation makes it easy to subtract any offset or background signal (remembering that at 650 °C the phosphor and its surroundings will likely be emitting detectable levels of thermal radiation) by subtracting the background when the LED is off from the signal when it is on. To reduce transient effects of the driver when the LED is switched on and the phosphor decay and amplifier time constant when the LED is switched off, measurements are gated to the shaded areas shown in figure 5, with the average 'off' signal subtracted from the average 'on' signal. The gating and timing are chosen such that the system is in a steady state when the measurements are
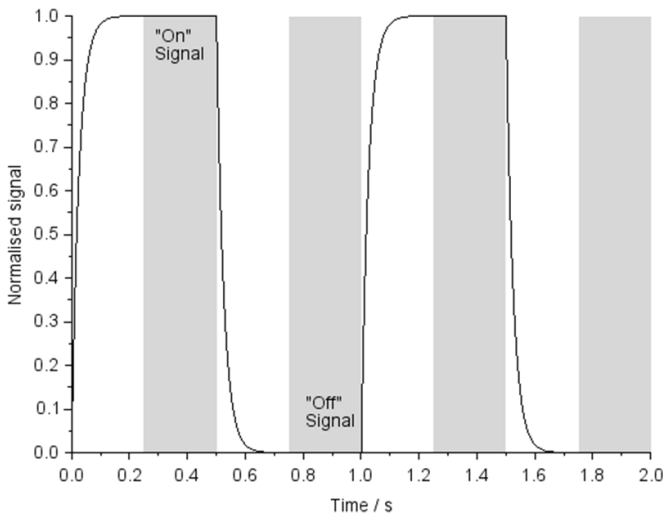
Figure 5. The phosphor is excited by the LED driven with a square wave at 1 Hz. Only photoluminescence data from the shaded areas are used, in this case measuring for 250 ms with the LED on and 250 ms with the LED off.
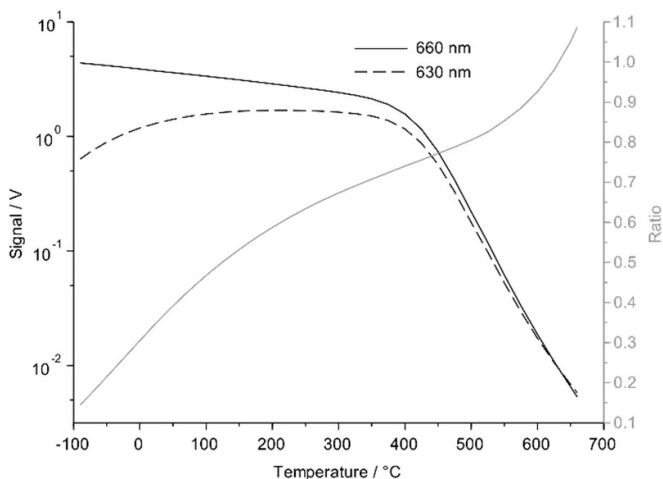

Figure 6. Signal levels from the two detectors (black lines and scale) and their ratio (grey line and scale).

made. In practice, only 50% of the data is used − shown as the shaded areas in figure 5—and this and the excitation frequency are kept the same for both calibration and use. The LED power is assumed to be fixed although some variation is allowed— and can be checked for with a power meter—and accounted for in the uncertainty budget. Therefore, for the calibration to be valid requires that the LED power is at this level and, also, that the square wave frequency and gating profile as given are used.

2.4. Range

The system was checked using an ice point, with a dry block calibrator up to 660 °C and in an oil bath down to −90 °C. The signal levels of the two channels (normalised to a gain of 10^7 VA^{-1}) and ratio are shown in figure 6.

3. Calibration

The required calibration range [3] was 0 °C to 650 °C, which was covered using an ice point and by comparison to a calibrated thermocouple using a dry well calibrator.

3.1. Thermocouple

Traceability to ITS-90 was with a type R thermocouple made from 0.5 mm diameter 2 m long pieces of thermocouple grade wire—nominally 99.99% purity—in 710 mm long twin-bore alumina. The wires were annealed for about 30 min in air at a minimum temperature of 1100 °C for the platinum wire and 1450 °C for the alloy wire. After making the junction the assembled thermocouple was annealed for about 30 min at 1100 °C.

The EMF of the thermocouple was measured at the freezing points of zinc and silver and the melting point of palladium-carbon eutectic. From these measurements a 3rd-order polynomial deviation equation was determined for the difference from the reference value calculated using the equations given in the relevant standards [14].

The standard uncertainty (i.e. $k = 1$) of the thermocouple calibration is estimated to be 0.15 °C from 0 °C to 1100 °C.

3.2. Dry block calibrator

A dry block calibrator (Ametek Jofra RTC-700) was used. This has a 210 mm deep insert with OD 29.8 mm and with 200 mm deep wells of various diameters. It has an operating temperature range from 33 °C to 700 °C. The unit's own temperature sensors are used to control the set point and maintain a constant value. Once the calibrator indicates its stability criteria have been reached, the EMF of the calibrated thermocouple is measured and converted to ITS-90 temperature using the relevant standard and deviation equation.

3.3. Method

The excitation voltage was set at 5 V as a square wave with a frequency of 1 Hz. The DAQ was set to make 100 000 readings per cycle. The data readings were gated as shown in figure 5. The EMF of the thermocouple was measured using a calibrated Datron 1271 digital voltmeter. The calibrated thermocouple and phosphor thermometer were each inserted inside closed end fused silica tubes 500 mm long with internal diameter 3 mm and 1 mm wall thickness.

An ice point—a mixture of crushed ice and deionised water in a Dewar flask that had been allowed to stabilise for 15 min or more—was used as a calibration point at 0 °C and for the cold junction of the calibrated thermocouple.

The phosphor probe and calibrated thermocouple were each placed in a well in the insert block of the calibrator. The system was taken to have reached stability when the dry-block calibrator was within a specified temperature limit at each set-point temperature (10 mK to 20 mK depending on the set-point temperature) for 10 min. The calibrated thermometer provided the ITS-90 temperature and a series of 10–20 measurements

of the intensity ratio was made. The calibrator set point was increased in 50 °C steps from 50 °C to 650 °C, and then stepped back in 50 °C steps to 50 °C. The phosphor probe was then re-measured in the ice point.

At some temperatures, measurements were made on two gain settings so that the gain ratios ($10^7/10^8$ and $10^8/10^9$) could be determined.

Two further repeat sets of measurements were made on subsequent days.

3.4. Evaluation

The detector signals of the two sensors were divided to give the intensity ratio. The difference in ratios using different gain settings on the detector amplifiers allowed gain setting corrections to be calculated, and all phosphor ratios were expressed as if on gain setting 10^7 VA^{-1}. Each phosphor ratio was equated to the ITS-90 temperature given by the calibrated thermocouple. A cubic spline interpolation to the calibration points was made using the LabVIEW *Interpolate 1D* function (VI).

3.4.1. Uncertainty of phosphor sensor calibration.
The most important aspect of assessing the thermometer is a comprehensive evaluation of the calibration uncertainty [15]. The following components were identified as contributing to the overall uncertainty at each calibration point.

3.4.1.1. Uncertainty of dry block calibrator, u1.
The temperature of the insert is determined using the calibrated type R thermocouple. The combination of the Jofra RTC-700 with calibrated type R as a calibration source had been previously assessed and, including a component for immersion uniformity, has a standard ($k = 1$) uncertainty of 0.205 °C.

3.4.1.2. Specification of dry block calibrator, u2.
As well as the uncertainty of the calibrated standard and its uniformity for varying depth of sensor immersion in the calibrator, an uncertainty component for the radial uniformity based on the manufacturer's specification was included (u2a). The stability as claimed by the manufacturer is also included (u2b).

In tests at NPL no significant differences were found between different wells in the block, and stability during immersion tests was always better than 5 mK. Given this evidence, we judge the manufacturer's claims to be conservative.

3.4.1.3. Repeatability, u3.
This is the standard deviation of repeated measurements made under the same nominal conditions, that is, repeated measurements made over three calibration cycles at the same set point temperature made during either heating or cooling.

3.4.1.4. Hysteresis, u4.
The average difference across the three cycles between measurements made during heating and measurements made during cooling. This is taken to be a

rectangular distribution and so the value is divided by $\sqrt{3}$. In addition, an assumption is made that the average of the heating and cooling will be used as the calibration value and so u4 is further divided by a factor of two.

If only one value is used, then u4 should not be divided by the additional factor of two.

3.4.1.5. Phosphor sensor measurement type-A, u5.
This is the standard deviation of the 10–20 measurements made at each calibration point.

3.4.1.6. Interpolation, u6.
There is no physical basis to the calibration spline, and no reason it should be correct between calibration points. To evaluate this, alternate calibration points were omitted from the spline. The calculated values at the omitted points were compared to the measurement values. The alternated calibration points were then swapped, and the process repeated. Since this gives interpolation errors based on 100 °C intervals, it overestimates the error. As the actual calibration interval was 50 °C, the calculated differences were halved to give u6. This component is a rectangular distribution: it has a value between zero at the calibration points and a maximum at some intermediate point. Provisionally, we take the mid-point—where the measurement was compared to the interpolation—as being the maximum and so u6 is further divided by $\sqrt{3}$.

3.4.1.7. Self-heating, u7.
There is a noticeable effect whereby if the sensor is thermally stabilised before the excitation is turned on, then when it is actuated the ratio changes as if the sensor temperature was increasing. Since this depends on the LED excitation level—it is a bigger effect at higher LED powers (excitation voltages)—it is taken to be due to a warming of the phosphor by absorption of the excitation light. Within the calibration range it is most noticeable at the ice point (as might be expected given the difference between the static ice point and the dynamically controlled, and heated, dry well calibrator). However, it has been allowed as a possible uncertainty throughout—scaled accordingly with the cubic-spline interpolation.

3.4.1.8. Connection, u8.
The fibre-to-fibre connection from the sensor to the measuring head is a potential source of uncertainty due to changes in transmission between measurement wavelengths. To evaluate this, a first ice-point measurement was made before the system was dismantled, moved and reassembled (including cleaning the fibre-to-fibre connection). A second ice-point measurement was found to be less than 50 mK different from the first. This value was propagated to other temperatures according to the cubic-spline interpolation.

3.4.1.9. Gain ratio, u9.
Nominally, the amplifier gains are set in decadal steps (10^7 VA^{-1}, 10^8 VA^{-1} and 10^9 VA^{-1} are used), but the actual intervals are slightly different from 10, and vary

Table 1. Uncertainty budget ($k = 1$) for the phosphor thermometer from 0 °C to 650 °C, showing which components contribute most to the overall uncertainty, U. All values have units of degree Celsius.

T	u1	u2a	u2b	u3	u4	u5	u6	u7	u8	u9	u10	u11	u12	u13	U
0	0.21	0.00	0.00	0.37	0.39	0.00	0.00	0.05	0.05	0.00	0.10	0.03	0.12	0.00	**0.60**
50	0.21	0.10	0.01	0.31	0.25	0.00	0.68	0.05	0.05	0.00	0.14	0.05	0.13	0.09	**0.86**
100	0.21	0.10	0.01	0.25	0.11	0.00	0.17	0.06	0.06	0.00	0.20	0.07	0.15	0.08	**0.48**
150	0.21	0.25	0.02	0.42	0.10	0.00	0.12	0.07	0.07	0.00	0.27	0.09	0.18	0.08	**0.66**
200	0.21	0.25	0.02	0.59	0.09	0.00	0.06	0.09	0.09	0.00	0.37	0.12	0.21	0.08	**0.83**
250	0.21	0.25	0.02	0.64	0.07	0.00	0.24	0.10	0.10	0.00	0.50	0.15	0.25	0.06	**0.97**
300	0.21	0.25	0.02	0.69	0.04	0.00	0.35	0.12	0.12	0.00	0.66	0.18	0.29	0.07	**1.14**
350	0.21	0.25	0.02	0.66	0.06	0.00	0.09	0.13	0.13	0.00	0.87	0.20	0.32	0.06	**1.22**
400	0.21	0.25	0.02	0.63	0.07	0.06	0.32	0.14	0.14	0.00	0.54	0.21	0.33	0.06	**1.05**
450	0.21	0.40	0.02	0.61	0.22	0.01	0.82	0.14	0.14	0.14	0.15	0.21	0.33	0.05	**1.24**
500	0.21	0.40	0.02	0.60	0.37	0.10	0.86	0.12	0.12	0.12	0.98	0.16	0.28	0.05	**1.59**
550	0.21	0.40	0.02	0.31	0.27	0.03	1.91	0.08	0.08	0.23	0.32	0.11	0.19	0.05	**2.06**
600	0.21	0.40	0.02	0.95	0.18	0.01	1.56	0.04	0.04	0.14	0.17	0.07	0.11	0.05	**1.90**
650	0.21	0.40	0.02	0.95	0.00	0.01	1.56	0.03	0.03	0.10	0.17	0.08	0.07	0.05	**1.89**

between the two detectors. This means that the intensity ratio of the thermometer changes slightly depending on the gain setting of the detectors (it is assumed that the same gain is used on both). The interpolation is based on all intensity ratios being at a gain 10^7 VA^{-1} equivalent. The uncertainty u9 allowing for the use of different gains is the standard deviation of the measurements used to determine the amplification changes from 10^7 VA^{-1} it is 0.000279 and for 10^9 VA^{-1}, 0.000302. This is expressed as temperature using the cubic-spline interpolation. In this case, 10^8 VA^{-1} has been applied to the calibration points 450 °C and 500 °C and 10^9 VA^{-1} applied to 550 °C, 600 °C and 650 °C.

3.4.1.10. DAQ: analogue input, u10. The NI 6356 DAQ specification allows the absolute accuracy of the analogue input to be determined (for example, it is 2.7 mV on ±10 V range). To evaluate this, the voltage uncertainty is added to the actual signal . The temperatures of the original and increased signals are calculated using the cubic spline and the temperature difference taken as the uncertainty. This is assessed with an assumption that the lowest range consistent with the two inputs is used (either ±1 V, ±2 V, ±5 V or ±10 V).

3.4.1.11. DAQ: analogue output, u11. The absolute accuracy of the analogue output is given as 1.6 mV at the 5 V output square wave signal from the DAQ. This fractional value is taken to be a rectangular distribution and treated in the same way as u10 allowed to propagate according to the cubic spline interpolation.

3.4.1.12. Excitation, u12. The phosphor intensity ratio is found to vary according to the level of excitation. It is noticeable that the LED driver has transient effects that distort the square wave output. The results here are based on keeping a fixed LED excitation at 5 V. Reducing this to 4.8 V changes the indicated temperature by 0.2 °C at 200 °C. This is accounted for as u12, scaled accordingly for other temperatures.

3.4.1.13. Voltmeter, u13. The Datron 1271 voltmeter used to determine the EMF of the calibrated thermocouple has an uncertainty of 0.6 μV on the 100 mV range used. This is expressed as an additional temperature uncertainty component in the source—multiplying this voltage uncertainty by the known sensitivity (μV K^{-1}) of type R thermocouples.

4. Calibration results

Based on using a cubic spline to evaluate temperature from the intensity ratio the uncertainty budget from 0 °C to 650 °C is given in table 1. The combined standard uncertainty, U, is the root-mean-square of the individual components.

The main contributors are; the repeatability and hysteresis of the sensor, the interpolation between calibration points and the absolute accuracy of the voltage measurement. The overall uncertainty at a coverage factor $k = 2$ (giving a coverage probability of approximately 95%) is shown in figure 7.

5. Discussion

We have endeavoured to give a sound metrological footing for the uncertainty that can be achieved for a phosphor-based contact probe using MFG. The wide temperature range (>700 °C) and relatively high emission intensity of this phosphor make it a good choice for thermometry. The principle of operation of a single fibre using the ratio of intensities up to 660 °C has been demonstrated and calibration uncertainties have been achieved that are small enough to be useful [3]. While it might be interesting to tie the calibration to the ITS-90 defined aluminium point at 660.323 °C, the thermometer uncertainties achieved here are too large to give this any practical advantage. Some of the dominant uncertainty components could be reduced, for example the interpolation uncertainty by having more calibration points and the gain ratio uncertainty by direct voltage measurement rather than indirect optical measurement.
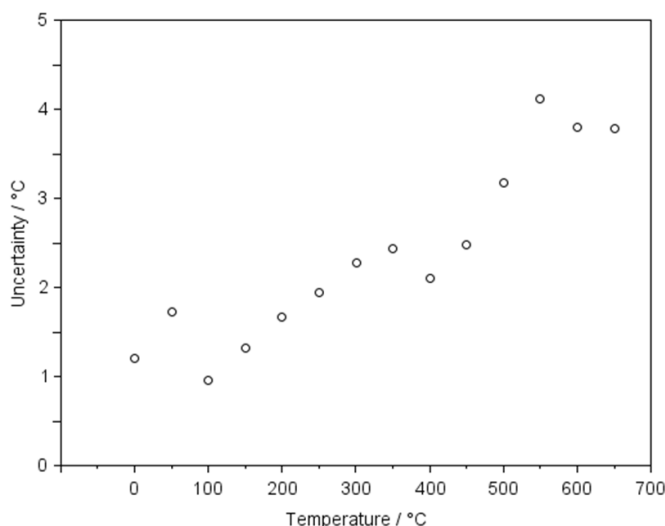
Figure 7. Uncertainty of calibration expressed at a coverage probability of approximately 95%.

Repeatability is also one of big contributors. It was found that with continued cycling to 650 °C the probe started to break-up. This is clearly a concern: a practical thermometer intended for use where more sensors cannot will have to operate successfully in a harsh environment. The need for a mechanically robust connection of fibre to phosphor was reported in [2], and they gave details of how they achieved this so it is a problem with a solution. In the meantime, we continue testing different bonding and encapsulation techniques using ceramics and ceramic glues. Preliminary results are that better robustness can be achieved, although at the expense of lower signal level.

Signal levels could be increased to compensate, but there are some limitations. If the need is for remote measurement, then extensive runs of large diameter multimode fibre become increasingly expensive for core diameters larger than the 400 μm used here. A dichroic mirror with a sharper cut-off near 645 nm can be obtained and this would increase the signal at the longer wavelength. This would be a useful improvement if higher temperatures were needed since, as can be seen in figure 6, the long wavelength signal starts to drop faster than the shorter wavelength above 650 °C. Multiple fibres could be used, separating the excitation and emission, but this would also increase the cost of long runs.

The system will next be tested in harsh environments: a plasma storm of charged particles and a 1 T magnetic field [3]. This will tell whether the phosphor probes can indeed work as thermometers where other devices fail.

6. Conclusion

A phosphor thermometer using the ratio of two wavelengths from the emission of manganese doped MFG phosphor excited with a blue light LED has been built. It has been shown to operate from −90 °C to 660 °C. The uncertainty components for a calibration traceable to ITS-90 have been evaluated for the sub-range 0 °C to 650 °C. The target uncertainty of 5 °C ($k = 2$) has been achieved. The uncertainty evaluation could allow such a thermometer to be part of a traceable calibration chain from sensor to national standards.

Data availability statement

The data that support the findings of this study are available upon reasonable request from the authors.

ORCID iDs

D Lowe https://orcid.org/0000-0003-1864-7139
G Sutton https://orcid.org/0000-0001-6753-2018
G Machin https://orcid.org/0000-0002-8864-6951
J Pearce https://orcid.org/0000-0003-1515-8815

References

[1] McSherry M, Fitzpatrick C and Lewis E 2005 Review of luminescent based fibre optic temperature sensors *Sensor Rev.* **25** 56
[2] Grattan K T V, Palmer A W and Zhang Z 1991 Development of a high-temperature fiber-optic thermometer probe using fluorescent decay *Rev. Sci. Instrum.* **62** 1210
[3] European Metrology Programme for Innovation and Research (EMPIR) Enhancing process efficiency through improved temperature measurement 2 *Project Number: 17IND04*
[4] Preston-Thomas H 1990 The International Temperature Scale of 1990 (ITS-90) *Metrologia* **27** 3
[5] Allison S W and Gillies G T 1997 Remote thermometry with thermographic phosphors: instrumentation and applications *Rev. Sci. Instrum.* **68** 2615
[6] Khalid A H and Kontis K 2008 Thermographic phosphors for high temperature measurements: principles, current state of the art and recent applications *Sensors* **8** 5673–744
[7] Aldén M, Omrane A, Richter M and Särner G 2011 Thermographic phosphors for thermometry: a survey of combustion applications *Prog. Energy Combust. Sci.* **37** 422
[8] Brübach J, Pflitsch C, Dreizler A and Atakan B 2013 On surface temperature measurements with thermographic phosphors: a review *Prog. Energy Combust. Sci.* **39** 37
[9] Abram C, Fond B and Beyrau F 2018 Temperature measurement techniques for gas and liquid flows using thermographic phosphor tracer particles *Prog. Energy Combust. Sci.* **64** 93–156
[10] Ali A, Khanzada L S, Hashemi A, Polzer C, Osvet A, Brabec C and Batentschuk M 2018 Optimization of synthesis and compositional parameters of magnesium

germanate and fluoro-germanate thermographic phosphors *J. Alloys Compd.* **734** 29

[11] Wagstaff F E and Richards K J 1966 Kinetics of crystallization of stoichiometric SiO$_2$ glass in H^{2}O atmospheres *J. Am. Ceram. Soc.* **49** 118

[12] Fiberguide industries (available at: www.fiberguide.com/product/high-temperature-fiber/)

[13] Aremco products inc (available at: www.aremco.com/high-temp-inorganic-binders/)

[14] IEC 60584-1 and BS EN 60584-1 2013. *Thermocouples. EMF specifications and tolerances*

[15] BIPM 2008 Evaluation of measurement data—guide to the expression of uncertainty in measurement (JCGM 100:2008) (BIPM)